

Degradation of resolution in a homogeneous dual readout hadronic calorimeter

Donald E. Groom

Lawrence Berkeley National Laboratory, 50R6008, Berkeley, CA 94720, USA

Abstract

If the response to a hadronic shower in a semi-infinite uniform calorimeter structure is S relative to the electronic response, then $S/E = [f_{em} + (1 - f_{em})(h/e)]$, where E is the incident hadron energy, f_{em} is the electronic shower fraction, and h/e is the hadron/electron response ratio. In conventional calorimeters the energy resolution is dominated by the stochastic variable f_{em} , whose broad, skewed pdf has an energy-dependent mean. The slow increase of the mean with E is responsible for response nonlinearity and the skewness results in a non-Gaussian response. If the cascade is observed in two channels with different values of h/e (typically scintillator(S) and Cherenkov(C)), f_{em} can be eliminated. An energy estimator, linear in C and S , is obtained which is proportional to the incident hadron's energy. The resolution depends upon the contrast in h/e between the two channels. The Cherenkov h/e will be 0.20–0.25. In sampling calorimeters, h/e can be increased to about 0.7 by arranging for preferential absorption of the electromagnetic (EM) shower energy in the absorber (decreasing e) and using a hydrogenous detector (organic scintillator) to enhance h through the contribution of recoil protons in n – p scattering. *Neither mechanism is available in a homogeneous crystal or glass scintillator*, where h/e is expected to be in the vicinity of 0.4 because of invisible hadronic energy loss and other effects. The h/e contrast is very likely too small to provide the needed energy resolution. We support this conclusion with simple Monte Carlo simulations.

Keywords: Hadronic calorimetry, hadron cascades, sampling calorimetry

PACS: 02.70.Uu, 29.40.Ka, 29.40.Mc, 29.40Vj, 34.50.Bw

1. Introduction

A homogeneous dual readout hadronic calorimeter has been proposed for a future linear collider. The machine will probably be an e^+e^- collider with a long bunch spacing (100's of ns), so that detectors with time constants in this range can be used. Discrimination between the Cherenkov signal (C) and scintillator

Email address: degroom@lbl.gov (Donald E. Groom)

(S) optical signals is expected to be made using a combination of timing and color.

In practice corrections must be made for cracks, leakage, and light collection variations, and the structure usually varies with depth. For the purposes of this analysis, however, we shall assume that the corrections have been made correctly, and consider a semi-infinite calorimeter with uniform structure that is either fine-sampling or homogeneous.

In each high-energy interaction in a hadronic cascade an average of $1/4$ of the energy is carried away by π^0 's[1]. These immediately decay to γ 's which initiate EM showers. This occurs many times, with the result that a large fraction f_{em} of the incident energy joins the EM shower. The mean, $\langle f_{em} \rangle$, is ≈ 0.5 for 100–150 GeV incident pions. It increases slowly with incident energy E , asymptotically approaching unity. Because of this energy dependence, the hadronic response is not linear in energy

The hadronic response S to an incident hadron is¹

$$S = E[f_{em} + (1 - f_{em})(h/e)] . \quad (1)$$

The EM energy deposit is detected with relative efficiency e , and the hadronic signal with relative efficiency h . Both vary from event to event. In part because of low multiplicities in the initial hadronic interactions, the variance of h is much larger than the variance of e . It makes sense to treat h/e as a stochastic variable; in Sec. 5 we treat it as Gaussian. The distribution of the more-usual e/h is fairly pathological.

Most energy deposit is by very low-energy electrons and charged hadrons. Because so many generations are involved in a high-energy cascade, the charged hadron spectra are essentially independent of the cascade's origin except for overall normalization. This “universal spectrum” concept is discussed in detail in Ref. [1]. It is because of this feature that $\langle h/e \rangle$ is a robust quantity, independent of energy and incident hadron species.

The energy-independent $\langle h/e \rangle$ does depend upon calorimeter composition and structure, as well as the readout—for example, an organic scintillator readout is sensitive to the otherwise-invisible neutron content of the cascade, and a Cherenkov readout is relatively blind to the hadronic content. $\langle f_{em} \rangle$ can be found by fitting the average π^-/e response as a function of test-beam energies with an appropriate $\langle f_{em} \rangle$ parameterization such as a power law in energy[1].²

If $\langle h/e \rangle$ is not unity, then the broad, skewed f_{em} probability distribution function (p.d.f.) significantly degrades and skews the energy resolution. It in fact usually dominates, producing the familiar wide, non-Gaussian energy distributions, as well as the non-linear response via its energy-dependent mean.

¹Here and elsewhere the energy E is normalized to the electron response.

²Technically, a power-law fit finds $a = (1 - \langle h/e \rangle)E_0^{1-m}$. Since $1 - m$ is small and the scale energy E_0 is close to 1 GeV for pion-induced cascades, the distinction is minor: $\langle h/e \rangle \approx 1 - a$. A similar distinction occurs when other parameterizations are used; h/e itself cannot be isolated.

If f_{em} could be *measured* for each event, then the response as given in Eq. 1 could be corrected to the actual energy with a much narrower Gaussian distribution with a mean proportional to the energy.

This was realized more than 3 decades ago, when the physics summarized in Eq. 1 was first understood. Schemes for measuring and correcting for f_{em} have been the object of discussion and experiment ever since.

Events in the high-energy tail of the distribution are EM-rich (with large f_{em}), since detection efficiency for the EM energy deposit is larger than for the hadronic deposit ($h/e < 1$). EM showers result in large local energy deposit; with sufficient readout segmentation this “lumpiness” provides a measure of f_{em} . This approach was used successfully by the WA1 collaboration[2], but has been less successful elsewhere, e.g., the ATLAS central barrel calorimeter[3].

An alternative is to obtain two signals for each event, one preferentially sensitive to the EM content (invariably Cherenkov readout) and one as sensitive as possible to the hadronic content (scintillator). This could be done either by readout of separate elements, as so successfully demonstrated by the DREAM collaboration[4], or by separation via color and timing information in a single material[5].

This study is motivated by renewed interest in the latter approach, in particular a homogeneous dual-readout heavy crystal (or glass) calorimeter for use at a future linear collider. The collider’s bunch spacing is to be in the 100–500 μ s range, a good match to the properties of many high- $\langle Z \rangle$ inorganic crystals and glasses. The hope is to separate the prompt Cherenkov pulse and the later, redder, scintillation pulse. A combination of timing, pulse shape, and color is to be used to resolve the Cherenkov and scintillation signals. This possibility is being successfully explored by Akchurin, et al.[6, 7].

While Akchurin et al. have demonstrated the desired signal separation in at least BGO and PbWO₄, I am concerned that low h/e for the scintillator component will prevent adequate hadronic energy resolution. In this paper I explore the likely resolution as a function of energy and $\langle h/e|_S \rangle$ using resolution contributions based on published homogeneous crystal and sampling calorimeter performance. Simple, transparent Monte Carlo’s (MC’s) are used by preference, to make the physics more transparent than if a sophisticated MC such as GEANT4 were used. The probability distribution function (p.d.f.) of f_{em} is approximated with some care, while other resolution contributions are taken to be Gaussian.

2. $\langle h/e \rangle$ in a high-density crystal or glass scintillator

In an EM cascade the electrons are relativistic until their energies fall well below the critical energy, so that almost all of the energy is deposited by near-minimum ionizing electrons. No appreciable energy exits from the EM cascade via photonuclear interactions. The result is a response very nearly linear in the incident electron or photon energy.

Hadronic interactions deposit energy in a variety of ways (See Table 1 [by Gabriel and Schmidt] in Ref. [8]; detailed discussions can be found in

Refs. [9, 10] and other recent reviews). A large fraction of the energy ($\approx 20\%$ for Fe/scintillator and $\approx 40\%$ for U/scintillator sampling calorimeters) goes to nuclear dissociation and is “invisible.” Some fraction of the neutrons can be detected via n - p scattering in hydrogenous materials such as organic scintillator, but much or most of the neutron energy is also lost. Low-energy protons and charged fission fragments produce saturated signals in scintillator[11].³ All of these factors result in low visible response to the hadronic component of the cascade relative to response to the EM component.

Detection of recoil protons in neutron scattering in hydrogenous detectors increases h [13]. In a sampling calorimeter a disproportionate fraction of the EM energy is deposited in the higher- Z absorber; the absorber/active region thickness ratio can be “tuned” to decrease e . Both of these effects increase h/e . In practical sampling calorimeters $\langle h/e \rangle$ is typically 0.7, and can be made to approach unity with careful design.

Neither mechanism for increasing h/e is available to a high-density homogeneous calorimeter.

As we shall see, the resolution is dependent on the “ h/e contrast,” the difference between $\langle h/e \rangle$ for the Cherenkov ($\langle h/e|_C \rangle$) and scintillation ($\langle h/e|_S \rangle$) readouts. Based on experience with quartz-fiber readout calorimeters[14–16], $\langle h/e|_C \rangle = 0.20$ – 0.25 .⁴ There are few data concerning $\langle h/e|_S \rangle$ in a homogeneous calorimeter, but there is no way to hide EM energy in absorber and there is very little neutron sensitivity. We might expect as much as 30% of the hadron energy to be expended on nuclear dissociation and therefore invisible, and 15%–20% to be carried by neutrons. These alone would result in $\langle h/e|_S \rangle \approx 0.5$. There are other effects, such as incomplete Cherenkov-scintillator separation and saturated scintillator response to highly ionizing particles, so $\langle h/e|_S \rangle = 0.35$ – 0.5 might be expected. This is corroborated by a comment in Ref. [7]: “The e/h value of ECAL [PbWO₄] as a scintillation device is much larger than for the Cu/plastic sampling structure in DREAM: 2.4 vs. 1.3.” ($h/e = 0.43$ vs 0.7.)

3. Dual-readout hadronic calorimetry

Nearly thirty years ago it was proposed that the nonlinearity and skewness engendered by f_{em} could be eliminated with a “dual-readout calorimeter”[18] with readouts having contrasting values of $\langle h/e \rangle$. The usual scenario is a Cherenkov readout (C) that is fairly blind to hadronic activity and a scintillator readout (S) with optimized hadronic response. Within the last decade the DREAM collaboration has elegantly implemented the proposal with a test-beam calorimeter having simultaneous quartz fiber and plastic scintillator fiber readouts[15–17, 19]. Eq. 1 is replaced by

$$S = E[f_{em} + (1 - f_{em})(h/e|_S)] \quad (2)$$

³This occurs in inorganic as well as organic scintillators[12].

⁴From the data shown in Table 3 of Ref. [14] I obtain $h/e|_C = 0.247$ [17].

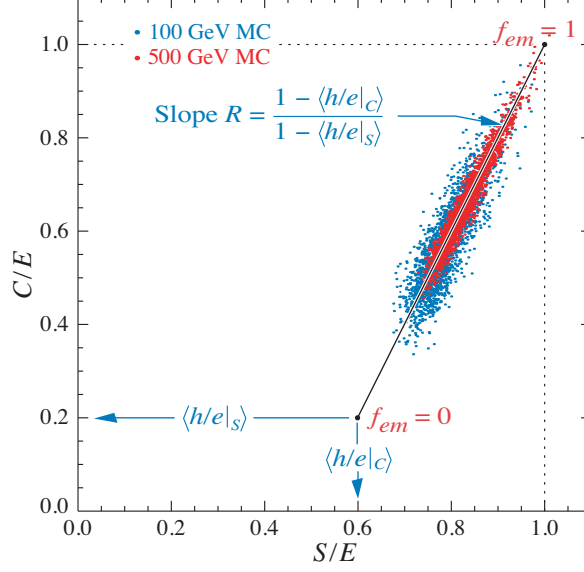


Figure 1: Energy-independent event locus in the C/E - S/E plane. With increased energy, resolution improves and the mean moves upward along the locus.

$$C = E[f_{em} + (1 - f_{em})(h/e_C)] . \quad (3)$$

In parametric form, Eqns. (4) and (5) describe a straight line-segment event locus in the C - S (or C/E - S/E) plane, as illustrated in Fig. 1. If the cascade is “all electromagnetic” ($f_{em} = 1$), then $S/E = C/E = 1$. If the cascade is “all hadronic” ($f_{em} = 0$), then $S/E = h/e|_S$ and $C/E = h/e|_C$. (The MC “events” shown in the figure are discussed below.) The slope in the C/E - S/E plane is independent of energy; with increasing energy the distribution just moves up along the locus.

It is convenient to introduce the less cumbersome notation $h/e|_X \equiv \eta_X$:

$$S = E[f_{em} + (1 - f_{em})\eta_S] \quad (4)$$

$$C = E[f_{em} + (1 - f_{em})\eta_C] \quad (5)$$

$$(6)$$

Equations (4) and (5), linear in $1/E$ and f_{em} , can be rewritten as

$$\begin{pmatrix} C & -(1 - \eta_C) \\ S & -(1 - \eta_S) \end{pmatrix} \begin{pmatrix} 1/E \\ f_{em} \end{pmatrix} = \begin{pmatrix} \eta_C \\ \eta_S \end{pmatrix} \quad (7)$$

with solutions

$$E = \frac{S(1 - \eta_C) - C(1 - \eta_S)}{\eta_S - \eta_C} \quad (8)$$

$$f_{em} = \frac{C\eta_S - S\eta_C}{S(1 - \eta_C) - C(1 - \eta_S)} . \quad (9)$$

There is an important difference between Eqs. 1, 2, and 4, and Eq. 8: The first three give estimators of the scintillator response, given $f_{em}, h/e, \eta_S$, and the incident energy E . In contrast, Eq. 8 provides an estimator of this energy given S, C, η_S and η_C .

In Eqs. 8 and 9, η_C and η_S are the values *peculiar to that event*. These are unknown—and unknowable, until some way of tagging the hadronic composition becomes available.⁵ But in an experimental situation, an estimator of the energy must be established for each event. There is little choice but to replace these quantities by their means.

In this case, it is convenient to write the energy estimator (Eq. 8) more compactly as

$$E = \frac{RS - C}{R - 1}, \quad (10)$$

where I have made use of the slope of the event locus (the ratio of ranges of S and C) shown in Fig. 1:

$$R \equiv \frac{1 - \langle \eta_C \rangle}{1 - \langle \eta_S \rangle} \quad (11)$$

If C and S are independent, the variance of the corrected energy is given by

$$\sigma_E^2 = \left(\frac{R}{R-1} \right)^2 \sigma_S^2 + \left(\frac{1}{R-1} \right)^2 \sigma_C^2 \quad (12)$$

where σ_S^2 and σ_C^2 are discussed in Sec. 5. This provides a limited check on the MC simulations.

4. Electromagnetic fraction

In a dual-readout calorimeter estimators of E and f_{em} can be determined on an event-by-event basis. Both are subject to fluctuations from other contributions to the resolution. The EM fraction f_{em} is no longer a stochastic quantity.

The f_{em} p.d.f. has an energy-dependent mean (near 0.5 at 100–150 GeV, approaching unity as $E \rightarrow \infty$). Its standard deviation is about 11%, depending weakly on energy and calorimeter composition, and it is skewed to the large- f_{em} side[9, 17]. The mean, fractional standard deviation, and standard deviation of f_{em} as simulated by FLUKA90⁶ for cascades in a large lead cylinder are shown in Fig. 2. For this case I obtain⁷

$$\langle f_{em} \rangle = 1 - \left(\frac{E}{0.76 \text{ GeV}} \right)^{1-0.87} \quad (13)$$

⁵Neutron detection has been proposed and is being explored for this purpose.

⁶Since FLUKA90 many improvements have been made, especially in the nuclear physics modeling. The high-energy cascade modeling is nearly the same. Only the π^0 energy fraction in the cascade is of interest here.

⁷These functions are entirely empirical, the only constraint being that $\langle f_{em} \rangle \rightarrow 1$ as $E \rightarrow \infty$.

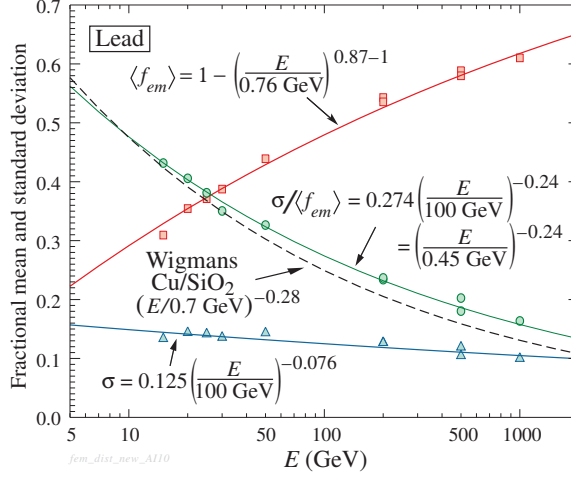


Figure 2: The mean, standard deviation, and fractional standard deviation of f_{em} in lead, as simulated by FLUKA90. This is basically Fig. 3(b) in Ref. [17]. An error in the fit to the fractional standard deviation has been corrected, a slightly different MC data set has been used, and Wigman's fit to the fractional standard deviation in a copper/quartz-fiber calorimeter has been added[9].

$$\sigma = 0.125 \left(\frac{E}{100 \text{ GeV}} \right)^{-0.076}. \quad (14)$$

The skewness $\gamma_1 (= \mu_3 / \sigma^3$, where μ_3 is the third moment about the mean) is not well-determined from our simulations, but it is about 0.6, which is assumed here. Although I use the above expressions for the present calculations, the exact form will be somewhat different for different calorimeter structures. The fractional standard deviation found for a copper/quartz-fiber calorimeter (Fig. 4.46 in Ref. [9]) is shown in Fig. 2 for comparison.)

In Ref. [17] it was pointed out that the Beta p.d.f.,⁸

$$B(x; \alpha, \beta) \propto x^{\alpha-1} (1-x)^{\beta-1}, \quad (15)$$

is very similar to the f_{em} p.d.f. with proper choice of α and β , except for the position of the mean. The mean, variance, and skewness are given by:

$$\mu = \frac{\alpha}{\alpha + \beta} \quad (16)$$

$$\sigma^2 \equiv \langle (x - \mu)^2 \rangle = \frac{\alpha\beta}{(\alpha + \beta)^2 (\alpha + \beta + 1)} \quad (17)$$

$$\gamma_1 \equiv \langle (x - \mu)^3 \rangle / \sigma^3 = \frac{2(\beta - \alpha) \sqrt{\alpha + \beta + 1}}{(\alpha + \beta + 2) \sqrt{\alpha\beta}} \quad (18)$$

⁸The normalization constant is the reciprocal of the Beta function $B(\alpha, \beta)$. For our purposes the p.d.f. is scaled to unity at the maximum.

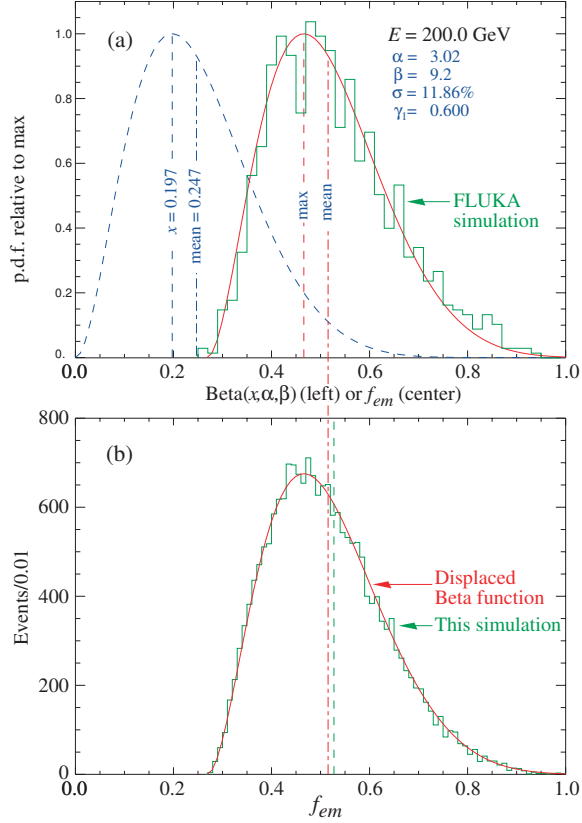


Figure 3: Approximation of the f_{em} p.d.f by a displaced Beta p.d.f. for 200 GeV pions incident on a lead “calorimeter.” (a) The Beta p.d.f. (dashed curve) with σ from Eq. 14 and $\gamma_1 = 0.6$, and the distribution displaced to the mean given by Eq. 13 (solid curve). The superimposed histogram is from a FLUKA simulation. (b) The same f_{em} distribution with a histogram of 20 000 MC events chosen from this p.d.f., compared with the displaced Beta function. The vertical dashed line show the means of the simulation.

To construct the p.d.f. for f_{em} , Eqns. 17 and 18 are solved for α and β , using σ as given by Eq. 14 and $\gamma_1 = 0.6$. The Beta p.d.f. is then displaced by $\langle f_{em} \rangle$ (Eq. 13) $-\mu$ (Eq. 16). Technically the displaced function does not go to zero at $x = 1$, but it is sufficiently close to zero that the problem can be ignored. The procedure is illustrated in Fig. 3(a) for $E = 200$ GeV in lead. The distribution from the FLUKA simulation is superimposed.

Values of f_{em} are chosen from the function by choosing uniformly distributed random points (f_{em}, y) and retaining the values of f_{em} when y is not above the p.d.f. at that value of f_{em} . The histogram of such a distribution is overlaid on the model p.d.f. in Fig. 3(b). These distributions are used for the present studies.

5. Resolution contributions

In a dual-readout calorimeter f_{em} has been elevated from a stochastic quantity to a measured quantity. In the absence of other resolution contributions, C and S are completely correlated, and the reconstructed energy distribution given by Eq. (8) or Eq. (10) is a delta function.

The signal distribution is broadened by photoelectron (p.e.) statistics, uncertain shower leakage corrections, uncorrected signal collection irregularities, electronic noise, sampling fluctuations (in the case of a sampling calorimeter), intrinsic fluctuations in the visible fraction of hadronic energy deposition, and other effects. As a matter of convenience in this discussion, I ignore the contributions from the readout-associated factors or assume that their contributions are lumped into $\sigma^{\text{p.e.}}$. Although published resolution measurements often involve constants and other deviations from $1/\sqrt{E}$ scaling, for our present purposes I use

$$\frac{\sigma_E}{E} = \frac{\sigma^{\text{p.e.}}}{\sqrt{E}} \oplus \frac{\sigma^{\text{intr}}}{\sqrt{E}} \oplus \frac{\sigma^{\text{samp}}}{\sqrt{E}}, \quad (19)$$

where the σ 's on the right side are fractional resolutions at 1 GeV if E is in GeV.

1. *Readout statistics.* Photomultipliers or avalanche photodiodes will likely be used to detect the scintillation and Cherenkov light. In this case Gaussian (Poisson) fluctuations with variance equal to the number of detected photons, and hence proportional to the energy, are added to the signals. The fractional uncertainty thus scales as $1/\sqrt{E}$.

Electromagnetic calorimeters provide guidance about obtainable resolution. Some of these are tabulated in Sec. 28.9.1 of Ref. [19]. Although fractional resolution as good as $2\%/\sqrt{E}$ has been obtained in scintillating crystal calorimeters, the best reported Cherenkov response in lead-glass EM calorimeters was 5%, for the OPAL endcap[20], corresponding to 400 p.e.'s/GeV. To maximize the number of photoelectrons collected, $\approx 45\%$ of the ends of the lead-glass blocks were covered by the PMT's. Such collection efficiency will probably not be possible with the proposed crystal calorimeter.

At the other extreme, the DREAM detector obtained $35\%/\sqrt{E}$ (8 p.e./GeV) with quartz fibers[21–23]. Future improvements are possible, for example by extending the UV response of the photodetectors and UV transmission of the radiators.

In this model study it is realistic to assume a middle ground, $\sigma_C^{\text{p.e.}} = \sigma_{0,C}^{\text{p.e.}}/\sqrt{C}$, where $\sigma_{0,C}^{\text{p.e.}} \approx 10\text{--}20\%$, or 100–25 p.e.'s/GeV.

In most of the dual homogeneous calorimeters under discussion, the Cherenkov and scintillator signals are to be separated by color and pulse shape. This requires that the scintillation signal is not large compared with the Cherenkov signal, say $\langle S \rangle = \xi^2 \langle C \rangle$, where ξ^2 is “a few.” We take $\xi^2 = 4$ in this study: $\sigma_{0,S}^{\text{p.e.}} = \sigma_{0,C}^{\text{p.e.}}/\xi$.

2. *Sampling and intrinsic fluctuations.* In a sampling calorimeter most of the energy is deposited in the absorber, and there are large fluctuations in the

Table 1: Examples of near-compensating sampling hadron calorimeters. For our present purposes some calorimeter structure variation and constant terms in the fitted resolution have been ignored.

Calorimeter	Passive	Active	Resolution	h/e	Reference
(Akesson et al.)	Cu, U/Cu, U	Scint (2.5mm)	$36\%/\sqrt{E}$	0.90	[26]
HELIOS	U (3 mm)	Scint (2.5 mm)	$34\%/\sqrt{E}$	0.984 ± 0.006	[27]
ZEUS FCAL	U (3.0/3.2 mm)	Scint (2,5/3.0 mm)	$35\%/\sqrt{E}$	1.03	[28, 29]
WA80	U (3 mm)	Scint (3 mm)	$67\%/\sqrt{E}$	0.89	[30]
(Drews, et al.)	Pb (10 mm)	Scint (2.5 mm)	$44\%/\sqrt{E}$	0.90 ± 0.01	[25, 31]
(Drews, et al.)	U (3.2 mm)	Scint (3.0 mm)	$36\%/\sqrt{E}$	0.99 ± 0.01	[25]
SPACAL	Pb (4 \times scint vol)	1 mm scint fibers	$30\%/\sqrt{E}$	0.87	[32, 33]
PCAL*	Pb [†] (10 mm)	Scint (3 mm)	$32\%/\sqrt{E}$	0.89	[34]

* $E \leq 6.8$ GeV.

† Every 6th plate is 16 mm thick Fe.

small fraction of the visible hadronic energy deposited in the active medium. A homogeneous calorimeter is not subject to these sampling fluctuations; in fact, this is an important reason for choosing it.⁹

Much of the hadronic energy deposit is invisible, going to nuclear disassociation, the production of unseen neutrons, etc., with consequent “intrinsic” fluctuations in the visible signal even if there is no absorber. In all but a few dedicated test-beam experiments, sampling and intrinsic fluctuations are inextricable. Drews et al.[25] studied the problem using compensated sandwich calorimeters with separate readouts for odd- and even- numbered layers. Since sampling fluctuations from layer to layer are independent, the *sum* of the odd- and even-layer signals, and their *difference* have the same variance. Signals from the intrinsic fluctuations are correlated between layers, so sums and differences could be used to separate sampling and intrinsic variances. ($\sigma^{\text{p.e.}} \approx 7\%/\sqrt{E}$ did not significantly broaden the responses.) In the case of lead plates, the sampling contribution was $(41.2 \pm 0.9)\%/\sqrt{E}$ and the intrinsic contribution was $(13.4 \pm 4.7)\%/\sqrt{E}$. In the case of uranium plates, the sampling contribution was $(31.1 \pm 0.9)\%/\sqrt{E}$ and the intrinsic contribution was $(20.4 \pm 2.4)\%/\sqrt{E}$. Lead is probably closest to compositions likely to be considered for the homogeneous calorimeter, so this result is relevant to the present discussion.

Since f_{em} fluctuations do not contribute in a compensating calorimeter (by definition of “compensating”), its resolution is the result of p.e., sampling, and

⁹Some suggested schemes, such as alternating lead glass Cherenkov planes with heavy glass scintillator planes[24], are totally active but only quasi-homogeneous. In these cases sampling fluctuations have some importance.

Table 2: Summary of resolution contributions. Reference values in the last column are used in Sec. 6.

Std dev	Value at E	Reference value	Optimistic value
$\sigma_C^{\text{p.e.}}$	$\sigma_{0,C}^{\text{p.e.}}/\sqrt{C}$	$\sigma_{0,C}^{\text{p.e.}} = 15\%$	$\sigma_{0,C}^{\text{p.e.}} = 5\%$
$\sigma_S^{\text{p.e.}}$	$\sigma_{0,C}^{\text{p.e.}}/\xi\sqrt{S}$	$\xi = 2$	$\xi = 10$
$\sigma_C^{\text{intr.}}$	$\sigma_{0,C}^{\text{intr.}} \langle \eta_C \rangle / \sqrt{E}$	$\sigma_{0,C}^{\text{intr.}} = 170\%$	$\sigma_{0,C}^{\text{intr.}} = 85\%$
$\sigma_S^{\text{intr.}}$	$\sigma_{0,S}^{\text{intr.}} \langle \eta_S \rangle / \sqrt{E}$	$\sigma_{0,S}^{\text{intr.}} = 11\%$	5.5%

intrinsic variations.¹⁰ Examples of near-compensating calorimeter resolution are shown in Table 1. We may take $\sigma_E = 35\%/\sqrt{E}$ as a representative “best case.” Drew et al.’s Pb-plate calorimeter achieved $44\%/\sqrt{E}$ (italicized line in Table 1). Scaling to this resolution, $\sigma_S^{\text{intr.}} \approx (35/44) \times 13.4\%/\sqrt{E} \approx 11\%/\sqrt{E}$. We adopt this as the fiducial scintillator intrinsic resolution for this study. If $\langle \eta_S \rangle \neq 1$, then $\sigma_S^{\text{intr.}} = 0.11 \langle \eta_S \rangle / \sqrt{E}$.

The standard deviation $\sigma_C^{\text{intr.}}$ of η_C is more problematical. Light produced by relativistic pions, with smaller contributions from other hadrons and electrons produced via nuclear γ -ray interactions, contribute a hadronic component to the Cherenkov response. The QFCAL[14] and DREAM[16] collaborations found $\langle \eta_C \rangle = 0.20$ – 0.25 . Since most of the scintillation signal is produced by nonrelativistic ionizing particles, η_S and η_C are nearly independent.

Typically about 35 (relativistic) π^\pm ’s are produced by a 100 GeV pion showering in Pb.¹¹ The fractional standard deviation is $1/\sqrt{35} = 0.17$ at 100 GeV, or $1.7/\sqrt{E}$. This broad distribution is scaled down by $\langle \eta_C \rangle = 0.20$ – 0.25 : $\sigma_C^{\text{intr.}} \approx 1.7 \langle \eta_C \rangle / \sqrt{E}$.

These results are summarized in Table 2. Typical distributions of η_S and η_C are shown in Fig. 4. Since the energy distributions reported for compensating calorimeter, e.g., as given in Table 1 are all consistent with Gaussian distribution, it is evidently valid to consider the distributions discussed in this section as Gaussian as well. This results in near-Gaussian energy-estimator distributions as reconstructed from S and C .

6. Simulation of the energy estimator distribution

Equation 10 and the equivalent Eq. 8 describe the estimator of incident pion energy as obtained from the observed scintillation and Cherenkov signals. We incorporate the resolution contributions discussed in Sec. 5 and summarized in

¹⁰This is not quite true. Suppose, for example, that $\langle h/e \rangle = 1$, and we select a subset of events for which h/e fluctuates to 10% below the mean, to 0.9. For these events S is sensitive to fluctuations of f_{em} . The *distribution* of h/e about unity thus introduces sensitivity to f_{em} .

¹¹Section 2.3.1.3 of Ref. [9].

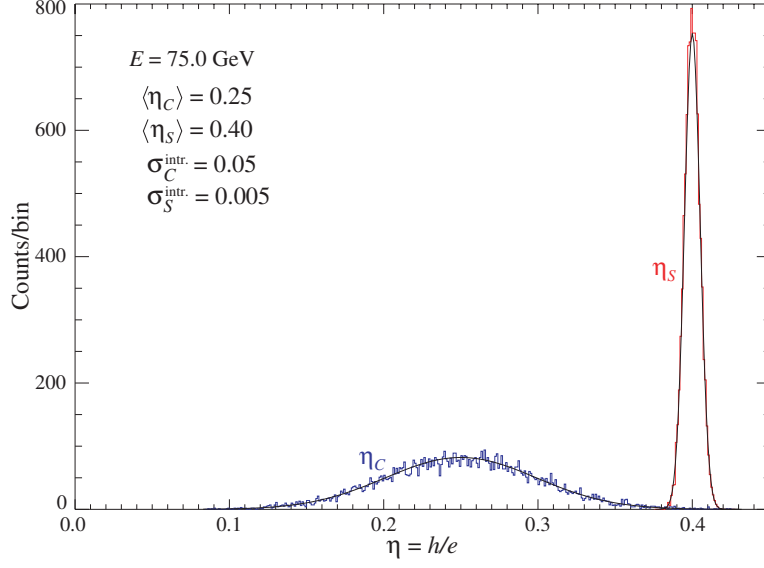


Figure 4: Input p.d.f.'s and MC realizations of the h/e distributions at 75 GeV for $\langle\eta_C\rangle = 0.25$ and $\langle\eta_S\rangle = 0.40$. $\sigma_S^{\text{intr.}}$ and $\sigma_C^{\text{intr.}}$ are from Table 2.

Table 2 to obtain distributions of S , C , and the energy estimator E via a simple, transparent Monte Carlo calculation as follows:

1. Choose the incident energy E and the detection efficiency ratios $\langle\eta_S\rangle$ and $\langle\eta_C\rangle$, fixing the latter in the range 0.20–0.25.
2. Choose the resolution parameters, using the reference values given in Table 2.
3. Generate an array of N values of f_{em} chosen from the displaced Beta distribution for energy E .
4. Generate N values of η_S from a normal distribution with mean $\langle\eta_S\rangle$ and fractional standard deviation $\sigma_S^{\text{intr.}}$. Similarly, generate N values of η_C from a normal distribution with mean $\langle\eta_C\rangle$ and standard deviation $\sigma_C^{\text{intr.}}$.
5. Construct the corresponding S and C arrays via Eqs. 4 and 5.
6. Replace each S and C as calculated in step 4 with values chosen from normal distributions with means S and C and standard deviations $\sigma_S^{\text{p.e.}}\sqrt{S}$ and $\sigma_C^{\text{p.e.}}\sqrt{C}/\xi$, respectively. The resulting S and C include p.e. statistics, and are used for subsequent “data analysis.” (Since $\sigma_S^{\text{p.e.}}$ and $\sigma_C^{\text{p.e.}}$ are fractional standard deviations, $\sigma_S^{\text{p.e.}}\sqrt{S}$ and $\sigma_C^{\text{p.e.}}\sqrt{C}/\xi$ have the same units as S and C (GeV).)
7. Find the energy estimator array via Eq. 8 or Eq. 10.

The results of four 10000 event simulations are shown in Fig. 5, at 75 and 200 GeV using realistic (0.4) and optimistic (0.6) values of η_S . In each case the mean value of the estimator of E (E_{est}) scaled by the beam energy is 1.00. The

Table 3: Parameters for the examples shown in Fig. 5, each based on 20 000 simulated events. In all cases $\eta_C = 0.25$.

	(a)	(b)	(c)	(d)
E_b	75 GeV	200 GeV	75 GeV	200 GeV
η_S	0.40	0.40	0.60	0.60
$\langle S/E_b \rangle$	0.67	0.71	0.78	0.81
σ_S	11.6%	10.1%	6.7%	5.9%
γ_{1S}	0.57	0.62	0.58	0.59
$\langle C/E_b \rangle$	0.59	0.64	0.59	0.64
σ_C	17.2%	14.2%	17.2%	14.2%
γ_{1C}	0.42	0.55	0.45	0.53
$\langle E_{\text{est}}/E_b \rangle$	0.999	1.000	1.000	1.000
σ_E	12.8%	7.24%	3.96%	2.27%
σ_E @ 1 GeV	111.%	102.%	34.3%	32.1%
γ_{1E}	0.008	0.002	-0.015	-0.003

distributions agree well with the Gaussians with the same mean and standard deviation drawn over the E histograms. In nearly all cases $|\gamma_1| \leq 0.05$, where γ_1 is the third moment about the mean divided by σ^3 .

The fractional standard deviation of the energy estimator scales as $1/\sqrt{E}$. The coefficient (resolution at 1 GeV) as a function of $h/e|_S (\equiv \eta_S)$ is shown in Fig. 6 for two values of $h/e|_C (\equiv \eta_C)$ that bracket the range found in SiO₂ calorimeters.

7. Discussion and conclusions

The standard deviations described in this section are highly uncertain, and can be used only as guides. The effect of large changes in the input variances on the resolution curves shown in Fig. 6 have been studied. Examples of optimistic excursions from best estimates are given in Table 2. At $\eta_S = 0.45$ and $\eta_C = 0.20$, where $\sigma_E = 52.5\%/\sqrt{E}$, the following improvements are found:

1. Increase the Cherenkov p.e. yield by a factor of nine, from $\sigma_{0,C}^{\text{p.e.}} = 15\%$ (44 p.e.'s/GeV) to $\sigma_{0,C}^{\text{p.e.}} = 5\%$ (400 p.e.'s/GeV). The resolution improves from $52.5\%/\sqrt{E}$ to $47.1\%/\sqrt{E}$, or -5.4% .
2. Increase the scintillator p.e. yield by a factor of 25 ($\xi = 2 \rightarrow \xi = 10$). The resolution improves from $52.5\%/\sqrt{E}$ to $49.0\%/\sqrt{E}$, or -3.5% . At least in this model, there is no serious penalty for using a “weak” scintillator.
3. Decrease the width of the Cherenkov intrinsic hadronic resolution at 1 GeV by a factor of two, from 170% to 85%. The former number is expected from fluctuations in the number of relativistic pions produced in the cascade, and so should be relatively dependable. However, this change produces a

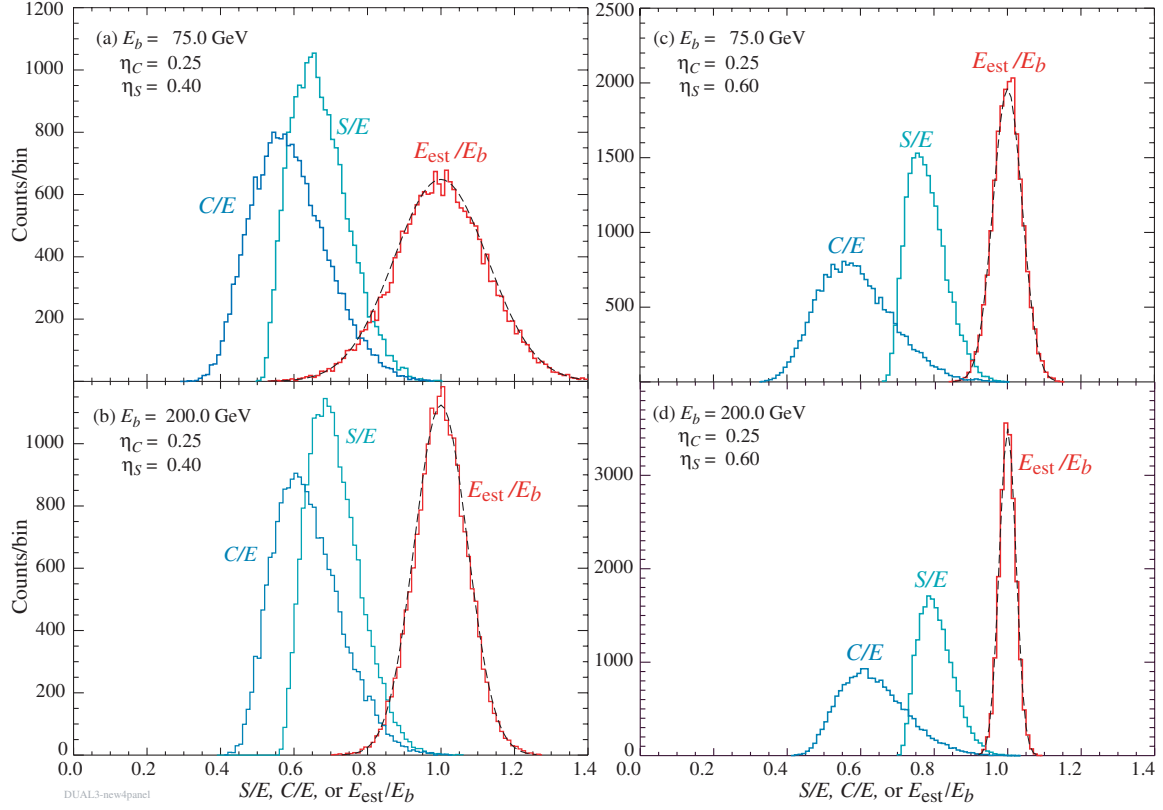


Figure 5: Monte Carlo distributions of C , S , and the estimator of E . (a) and (c) are for beam energies of 75 GeV; for (b) and (d) the beam energy is 200 GeV. For (a) and (b) $\eta_S = 0.40$, while for (c) and (d) $\eta_S = 0.60$. In all cases $\eta_C = 0.25$. Gaussians with the “measured” σ_E and mean relative to beam energy are shown as dotted black lines. Details are given in Table 3.

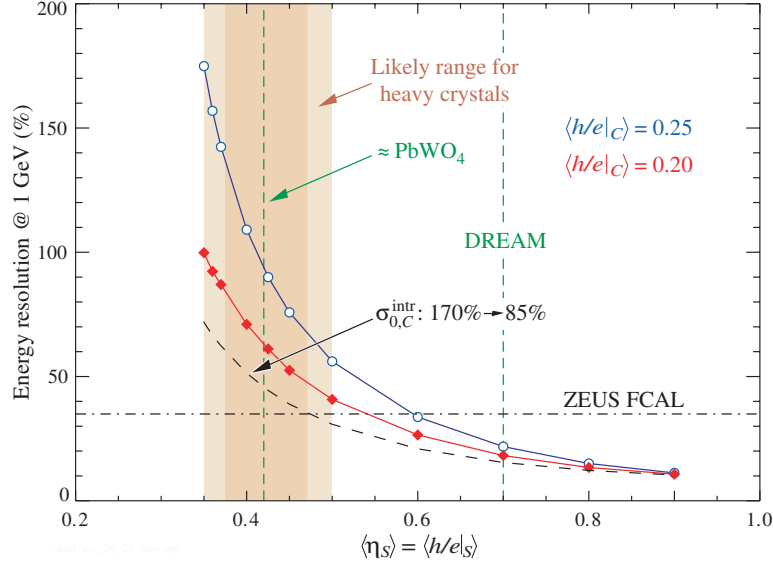


Figure 6: Dependence of resolution on η_S at two values of $\eta_C \equiv h/e|_C$. The results for $\eta_C = 0.20$ are essentially those for $\eta_C = 0.25$ displaced to the left by 0.05; it is the *contrast* between η_C and η_S that determines the resolution. The dashed line shows the effect of halving the width of the η_C p.d.f. The ZEUS FCAL resolution is typical for a compensated sampling calorimeter; see Table 1.

large improvement: $52.5\%/\sqrt{E} \rightarrow 39.1\%/\sqrt{E}$, or -13.4% . The curve for this case has been added to Fig. 6.

4. Finally, halve the width of the scintillator intrinsic hadronic resolution from $11\%/\sqrt{E}$ to $5.5\%/\sqrt{E}$. As expected, there is little effect: $52.5\%/\sqrt{E} \rightarrow 52.1\%$, or -0.4% . A substantial downward excursion of this number would be unlikely

The overall conclusion remains and is evident from Eq. 8: in a homogeneous hadronic calorimeter with dual readouts and a non-hydrogenous scintillator, event-to-event fluctuations of η_C and η_S destroy the resolution if their means are close. A large contrast between them is unlikely because the mechanisms that increase $\langle \eta_S \rangle$ are not present. It remains true that the mean of the energy estimator distribution is the beam energy, and its distribution is Gaussian.

Detailed simulations with a modern, sophisticated Monte Carlo program such as Geant4 would be desirable before commitment to a large R&D effort. It would be particularly informative to understand the means and variances of η_C and η_S .

Acknowledgments

I particularly thank Adam Para for getting me interested in this problem. Richard Wigmans' book, many papers, and many personal interactions have

been invaluable, as have been discussions with John Hauptman. The understanding of hadronic calorimetry underlying this paper has been slowly forged over at least the past 40 years by the insights and hard work of experts too numerous to mention.

This work was supported by the U.S. Department of Energy under Contract No. DE-AC02-05CH11231.

References

- [1] T.A. Gabriel, D.E. Groom, P.K. Job, N.V. Mokhov, G.R. Stevenson, Nuclear Instruments and Methods in Physics Research Section A 338 (1994) 336.
- [2] H. Abramowicz, et al., Nuclear Instruments and Methods 180 (1981) 429.
- [3] V.V. Abramov, et al., Nuclear Instruments and Methods in Physics Research Section A 457 (2001) 75.
- [4] R. Wigmans, Nuclear Instruments and Methods in Physics Research Section A 572 (2007) 215.
- [5] D. R. Winn, W. A. Worstell, IEEE Transactions on Nuclear Science 36 (1989) 334.
- [6] Akchurin, et al., Nuclear Instruments and Methods in Physics Research Section A 550 (2005) 185; Nuclear Instruments and Methods in Physics Research Section A 595 (2008) 359; Nuclear Instruments and Methods in Physics Research Section A 598 (2009) 710; Nuclear Instruments and Methods in Physics Research Section A 604 (2009) 512; Nuclear Instruments and Methods in Physics Research Section A 621 (2010) 212.
- [7] Akchurin, et al., Nuclear Instruments and Methods in Physics Research Section A 584 (2008) 273.
- [8] C.W. Fabjan, et al., Nuclear Instruments and Methods 141 (1977) 61; T. A. Gabriel, W. Schmidt, ORNL/TM-5105 (1975).
- [9] R. Wigmans, Calorimetry: Energy Measurement in Particle Physics, in: International Series of Monographs on Physics, vol. 107, 2000, pp. 1–726, Oxford University Press (2000).
- [10] C. Leroy, P.-G. Rancoita, Principles of Radiation Interaction in Matter and Detection, World Scientific (2004).
- [11] See fig 3.25, p. 145 in Ref. [9].
- [12] W. Moses, IEEE Transactions on Nuclear Science NS-55 (2008) 1049; W. Mengesha, et al., IEEE Transactions on Nuclear Science 45 (1998) 456.

- [13] Y. Galaktionov, et al., Nuclear Instruments and Methods in Physics Research Section A 251 (1986) 258.
- [14] N. Akchurin, et al., Nuclear Instruments and Methods in Physics Research Section A 399 (1997) 202.
- [15] R. Wigmans, “First results of the DREAM project,” in: Proceedings of 11th International Conference on on Calorimetry in Particle Physics, Perugia, Italy, 29 March–02 April, 2004, ed. C. Cecchi, P. Cenci, P. Lumbrano, M. Pepe, World Scientific (2005) 241.
- [16] N. Akchurin, et al., Nuclear Instruments and Methods in Physics Research Section A 537 (2005) 537.
- [17] D.E. Groom, Nuclear Instruments and Methods in Physics Research Section A 572 (2007) 633.
- [18] P. Mockett, A review of the physics and technology of high-energy calorimeter devices, in: Proceedings of 11th SLAC Summer Institute on Particle Physics, July 1983, SLAC Report No. 267 (July 1983).
- [19] J. Beringer, et al. (Particle Data Group), Physical Review D 86 (2012) 010001.
- [20] OPAL collaboration, Nuclear Instruments and Methods in Physics Research Section A 305 (1991) 275.
- [21] N. Akchurin, et al., Nuclear Instruments and Methods in Physics Research Section A 533 (2004) 305.
- [22] N. Akchurin, et al., Nuclear Instruments and Methods in Physics Research Section A 536 (2005) 29.
- [23] N. Akchurin, et al., Nuclear Instruments and Methods in Physics Research Section A 550 (2005) 185.
- [24] T. Zhao, “Active Absorber Calorimeter,” Contribution 119 at Linear Collider Workshop 2006, Bangalore, India (8–13 March 2006); indico.cern.ch/contributionDisplay.py?contribId=119&sessionId=5&confId=568
- [25] G. Drews, et al., Nuclear Instruments and Methods in Physics Research Section A 335 (1990) 335.
- [26] T. Akesson, et al., Nuclear Instruments and Methods in Physics Research Section A 241 (1985) 17.
- [27] T. Akesson, et al., Nuclear Instruments and Methods in Physics Research Section A 262 (1987).

- [28] A. Anderson, et al., Nuclear Instruments and Methods in Physics Research Section A 309 (1991) 101.
- [29] www-zeus.desy.de/bluebook/ch05/subsection2_4_15_3.html.
- [30] G. R. Young, et al., Nuclear Instruments and Methods in Physics Research Section A 279 (1989) 503.
- [31] E. Bernardi, et al., Nuclear Instruments and Methods in Physics Research Section A 262 (1987) 229.
- [32] D. Acosta, et al., Nuclear Instruments and Methods in Physics Research Section A 308 (1991) 481.
- [33] T. A. Armstrong, et al., Nuclear Instruments and Methods in Physics Research Section A 406 (1998) 227.
- [34] D. Fox, et al, Nuclear Instruments and Methods in Physics Research Section A 317 (1992) 474.